11th International Symposium on Turbulence and Shear Flow Phenomena (TSFP11)
Southampton, UK, July 30 to August 2, 2019

THE QUIESCENT CORE OF TURBULENT PIPE FLOW

Xue Chen
School of Engineering
University of Warwick
Coventry, CV4 7AL, UK.
x.chen.29@warwick.ac.uk

Yongmann M. Chung
School of Engineering
University of Warwick
Coventry, CV4 7AL, UK.
y.m.chung@warwick.ac.uk

Minping Wan
Department of Mechanics and Aerospace Engineering
Southern University of Science and Technology
Shenzhen, 518055, China.
wanmp@sustc.edu.cn

ABSTRACT

This study investigates the quiescent core region in turbulent pipe flow using direct numerical simulation (DNS). The quiescent core is a region with relatively constant and high momentum near the pipe centreline, and is identified from the probability density functions (*pdf*) of instantaneous streamwise velocity. The characteristics of the core and its interface are studied through conditional averages via multiple threshold velocities. The quiescent core expands in a hierarchical structural organisation as the velocity threshold decreases. The core displays significant meandering, thickening and thinning as found in channel flow. The intermittency is found to be smaller at the pipe centre compared to the channel, suggesting a stronger wall effect in the pipe flow. The core interface in the pipe flow shows several characteristics in common with the channel and boundary-layer flows: the streamwise velocity is relatively constant and change sharply across the interface with peaked vorticity. The magnitude of streamwise velocity jump is a function of distance from the wall, being larger near the wall. The core interface is found to be populated by strong azimuthal vortices, with most of them being prograde vortices.

INTRODUCTION

The quiescent core in pipe and channel, referring to the innermost uniform momentum zone (UMZ) near the centreline is an instantaneous phenomenon that has been found in the presence of wall-bounded flows. The existence of UMZs was first found in the experiment of turbulent boundary layer (TBL) by Meinhart & Adrian (1995), who observed irregularly shaped UMZs with marked sizes. The streamwise velocity is relatively constant in each zone and changes sharply at the interfaces where high shear and strong vorticity demarcate different zones. Adrian *et al.* (2000) reported that the TBL was densely populated by streamwise aligned thin structures with high vortical density in which enveloped regions of relatively constant streamwise velocity, namely the UMZs. These coherent structures formed in a hierarchical scale along the wall-normal direction across most of the turbulent boundary layer. Later, de Silva *et al.* (2016) confirmed the presence of UMZs in particle image velocimetry (PIV) data of TBL and observed an increase in zonal thickness for zones further away from the wall with a hierarchical length-scale distribution matching the observations by Adrian *et al.* (2000). de Silva *et al.* (2016) conducted conditional average analysis for the characteristics of the UMZs. Across all UMZ interfaces, sharp step-like changes in streamwise velocity were found and so as in other recent studies on TBL including Eisma *et al.* (2015) and Saxton-Fox & McKeon (2017). de Silva *et al.* (2017) found that the magnitude of the velocity jump across the interfaces is a function of wall-normal distance, being larger nearer the wall. Recently, Laskari *et al.* (2018) studied the time evolution of UMZs in TBL in which new UMZs were found to be originating from the wall, adding high momentum deficit into the log region where large-scale ejection events and a significant increase in turbulent activities were seen.

In turbulent channel flow, a single UMZ namely the quiescent core region was studied by Kwon *et al.* (2014) for a core defined at a fixed threshold velocity u_κ of $0.95U_{CL}$, 95% of the centreline velocity. The threshold velocity u_κ was obtained via the probability density function (*pdf*) of all the modal velocities extracted from the peaks on the histograms of instantaneous streamwise velocity which indicates large region with relatively small velocity dispersion. The core defined at $u_\kappa/U_{CL} = 0.95$ was found to be very large, covering roughly $\frac{3}{4}$ of the channel height. The quiescent core displays significant meandering, thickening and thinning behaviour and can penetrate very close to the walls, matching observations in Antonia *et al.* (1992) which found that the flow originated from one wall could penetrate to the near-wall region of the opposite wall of the channel. The meandering core occasionally leave the centreline outside with a overall intermittency of 7%. Yang *et al.* (2016) observed a strong distribution density of prograde spanwise vortices along with locally minimised retrograde vortices across the quiescent core interface in the turbulent channel flow. They also investigated the length of the core interface in the streamwise and spanwise directions and found that the core interface folds back and forth more intensely in the spanwise direction.

Studies on the single quiescent core in the pipe flow (Yang *et al.* (2017); Kwon (2016)) confirmed similar behaviour of the core to the channel. To bridge the gap between multiple UMZs studied for TBL and the quiescent cores in pipe and channel, this is the first study investigating the characteristics of multiple cores defined at different velocity thresholds. The structure arrangement of the multiple cores and the conditional averages across the core interface are presented in the results section. The contortion of the core interface and its correlation with the vortical structures are also visualised for multiple quiescent cores.

NUMERICAL METHOD

The direct numerical simulation (DNS) data of a fully-developed turbulent pipe flow at a friction Reynolds number $Re_\tau = 500$ are generated by a massively paralleled MPI spectral element (SEM) code, Nek5000 (Fischer *et al.* (2008)). A third-order semi-implicit time scheme solves the viscous terms implicitly using backward differentiation (BDF3) and the non-linear terms by extrapolation (EXT3). The periodic boundary condition was applied in the streamwise direction and the no-slip condition at the pipe wall. The computational domain of the $30R$-long pipe (R is the pipe radius) has 2652×314 elements, where each of the Gauss-Lobatto-Legendre (GLL) node has a Lagrange polynomial order of $N = 7$ for velocity and $N = 5$ for pressure known as $P_N - P_{N-2}$, resulting in a total number of 4.26×10^8 grid points for the velocity field similar to El Khoury *et al.* (2013). The pipe is meshed in the Cartesian coordinate to remedy the singularity issue on the centreline Jung & Chung (2012). In this study, the streamwise, azimuthal and radial directions of the pipe are denoted by x, θ and r respectively, with wall-normal distance $y = R - r$. The velocity components U, V and W are in the streamwise, vertical and horizontal directions in the Cartesian coordinates respectively. The wall-normal velocity in the radial direction is denoted as V_r. The orthogonal streamwise mid-planes have 393 grid points in the radial direction with resolution varies between $\Delta y^+ = 0.16$ and $\Delta y^+ = 4.24$. The resolution in the streamwise direction varies between $\Delta x^+ = 3.06$ and $\Delta x^+ = 9.99$. A grid independence test was reported in Wang *et al.* (2018).

RESULTS & DISCUSSION

Identification of the quiescent core

To identify the instantaneous UMZs, a detection technique developed by Kwon *et al.* (2014) and extended by Laskari *et al.* (2018) is used. The peaks on each instantaneous *pdf*s of streamwise velocity U are extracted as modal velocities from individual snapshots with a streamwise window size of $0.2R$. 110 bins for $U/U_{CL} \in [0, 1.1]$ with bin size 1% of U_{CL} are used, followed by a peak-detection scheme with constraints of a minimum distance between two peaks $F_d = 3\%$ of U_{CL}, a minimum height for peaks $F_h = 0.5\%$ (peaks with bin count less than 0.5% of total bin count are ignored) and a minimum prominence of the peak $F_p = 25\%$. Figure 1(a) shows an example of an instantaneous *pdf* of U from a selected snapshot. The two highest modal velocities are marked by arrows. The interfaces between the peaks are marked with dashed lines at $u_\kappa/Ucl = 0.95$ and 0.79. Figure 1(b) shows an cross stream plane from the same snapshot. The contours of U shows that the core region with the highest modal velocity bounded by the iso-surface of $u_\kappa/Ucl = 0.95$ (black contour) is significantly asymmetric is almost absence from quadrant 2. However, a large core region defined at a lower velocity threshold, $u_\kappa/Ucl = 0.79$ (white contour) is fairly uniformly distributed in all four quadrants, contributing a significantly enlarged area for velocity $0.79 < U/U_{CL} < 0.95$ in quadrant 2. This corresponds to the *pdf* in figure 1 where the peak at $0.95U_{CL}$ is lower than the peak at $0.79U_{CL}$. The same rationale explains the amplified region at $0.79 < U/U_{CL} < 0.95$ in the *pdf* of quadrant 2 only in figure 1(a).

Figure 2 shows the *pdf* of all modal velocities obtained from the instantaneous *pdf*s of U using all available snapshots. The fixed threshold velocity (u_κ) for cores are interpolated at the bin with the minimum bin count between neighbouring peaks. A fixed velocity threshold of $u_\kappa = 0.9U_{CL}$ extracted from figure 2 is used to study the characteristics of the quiescent core in a turbulent pipe flow. In order to investigate the behaviours of multiple quiescent core/UMZs, threshold velocity $u_\kappa/U_{CL} = 0.8$ and 0.7 bounding the three minor peaks marked in figure 2 are also used in the conditional average analysis. In addition, $u_\kappa/U_{CL} = 0.95$ used in studies on the quiescent core of channel and pipe (Kwon *et al.* (2014); Kwon (2016); Yang *et al.* (2016, 2017)) is also included for direct comparison.

Core location and thickness

The distance of the core interface from the pipe centre is denoted as r_κ so that $1 - r_\kappa$ represents the wall-normal distance of the core interface. In figure 4, the time-averaged (half) core thickness, r_κ increases as the velocity threshold decreases. The rate of change in r_κ is more rapid for cores defined at lower u_κ, being closer to the wall. The profile of r_κ indicates that cores at varying u_κ is not uniformly distributed between the centreline and the pipe wall but are more closely populated nearer the wall. Therefore, the gap between each core at lowering u_κ when approaching closer toward the wall decreases, forming a hierarchical structural organisation similar to the TBL (de Silva *et al.* (2016)).

The quiescent core show significant meandering and can leave the centreline outside the core. The intermittency of the quiescent core in the pipe flow is defined in the same way as in Kwon *et al.* (2014) for the channel flow. The intermittency factor $\gamma(r)$ represents the proportion of time that the flow spends outside of the core. $\gamma(r)$ is averaged in the streamwise and azimuthal directions and in time. Figure 5(a) shows that the near-wall flow ($r \to 1$) stays out of the core at all times, whereas the flow at the pipe centreline ($r = 0$) spends approximately 5% and 0.3% of the time outside the cores defined at $u_\kappa/U_{CL} = 0.95$ (red) and 0.9 (black), respectively. In figure 5(b), the centreline intermittency $\gamma(r = 0)$ for cores defined at varying velocity threshold u_κ decreases log-linearly. Cores defined at threshold velocities $u_\kappa < 0.9U_{CL}$ are found with zero centreline intermittency as they are naturally thicker. The centreline intermittency of channel flow in Kwon *et al.* (2014) was $\gamma \approx 6 - 8\%$ for at $u_\kappa/U_{CL} = 0.95$ (marked with a black square) for varies Reynolds number, slightly higher than pipe. This suggests that pipe flow is less intermittent due to the enclosed wall geometry.

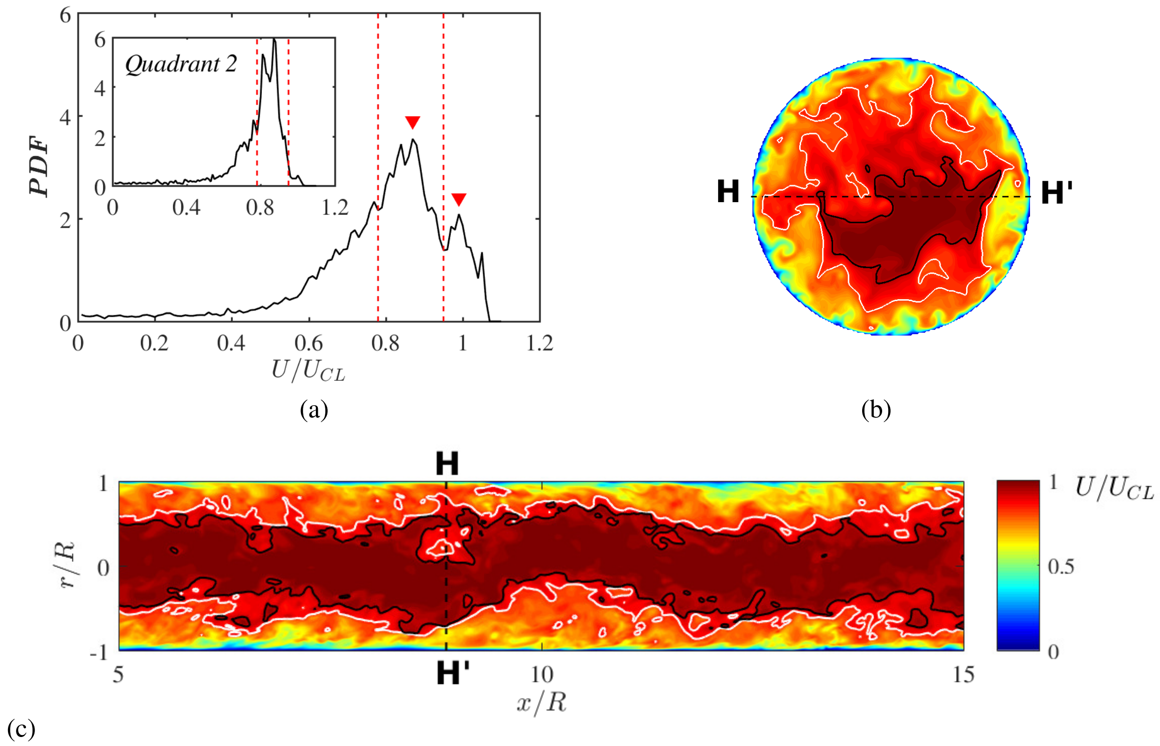

Figure 1. (a) Instantaneous *pdf*s of streamwise velocity U for a single snapshot using all vectors in the three-dimensional domain with a streamwise window size of $0.2R$. The *pdf* in the sub figure uses data points in the quadrant 2 only. (b) The quiescent core defined by $u_\kappa/U_{CL} = 0.95$ (black) and 0.79 (white) on the cross-stream plane with contour of U from the same snapshot as in (a). (c) Contour of U on the horizontal mid-plane from the same snapshot as in (a,b). The streamwise location marked by H and H' corresponds to the cross-stream plane in (b). The colour axis in (b,c) is the same.

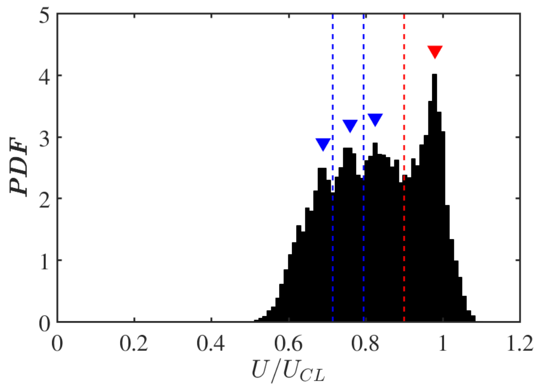

Figure 2. Time-averaged *pdf* of the modal velocities extracted as detected peaks on the instantaneous *pdf*s of U for all available snapshots.

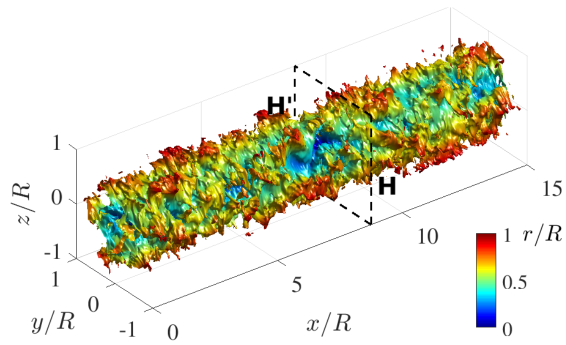

Figure 3. A three-dimensional quiescent core defined at $u_\kappa/U_{CL} = 0.9$ with colour based on core interface radius using the same snapshot as in figure 1. The cross-stream box marked by H and H' corresponds to the streamwise location chosen in figure 1(a) where significant meandering of the core is visualised.

Core interface characteristics

Figure 6 shows the conditionally averaged streamwise velocity $\langle U \rangle$ and azimuthal vorticity $\langle \Omega_\theta \rangle$ as functions of the distance from the core interface in the wall-normal direction, ξ. In figure 6(a), $\langle U \rangle$ exhibits a sharp change across the interface at $\xi = 0$ for both cores defined at $u_\kappa/U_{CL} = 0.9$ and 0.95, consistent with findings in the channel and TBL (Kwon *et al.* (2014); de Silva *et al.* (2016); Yang *et al.* (2016, 2017)). When the flow approaches the interface from outside the core ($\xi < 0$), $\langle U \rangle$ increases slowly up to the near-vicinity of the interface where $\langle U \rangle$ experiences a sudden increase across the interface. Inside the core, $\langle U \rangle$ is almost constant with a much smaller slope. The magnitude of the jump ΔU across the interface is defined following Yang *et al.* (2016) and is illustrated in figure 6(a). Figure 6(c) shows $\langle U \rangle$ for core defined at five u_κ values. The magnitude of jump in U across the interface is a function of u_κ, being larger for cores closer to the wall when defined at lower threshold velocities. Similar behaviour was found in TBL by de Silva *et al.* (2017) where the sharp step change in $\langle U \rangle$ at the edge of UMZs showed their magnitudes as a

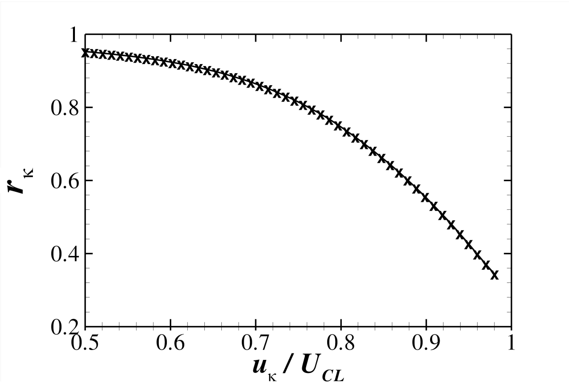

Figure 4. Averaged core interface radius equivalently half core thickness for cores defined at velocity threshold $0.5 \leq u_\kappa \leq 0.98$. $1 - r_\kappa$ represents the wall-normal distance of the core interface.

function of wall-normal distance. As further evidence for the cores being closer to each other near the wall, profiles of $\langle U \rangle$ for $u_\kappa/U_{CL} < 0.9$ show a preliminary jump (dashed part of coloured profiles at around $\xi \approx -0.1$). This preliminary jump can be interpreted as the interface of a neighbouring UMZ closer to the wall. Moreover, the location of this preliminary jump becomes closer to the main jump (at $\xi = 0$) as u_κ decreases, further supporting the hierarchical structural distribution of UMZs.

The step-like jump in figures 6(a,b) takes place over a thin layer of $-0.1 < \xi < 0.1$, indicating that the core interface itself has a thickness as found in the channel ((Yang *et al.*, 2016)) and TBL (de Silva *et al.* (2017)). In figure 6(b), this thin layer appears to be thinner nearer the wall for interfaces defined at lower u_κ. Figure 6(d) shows the velocity gradient $d\langle U \rangle / d\xi$. Cores closer to the wall with lower u_κ values have much larger $d\langle U \rangle / d\xi$ at the interface. Following Kwon *et al.* (2014), the interface thickness can be estimated as $\Delta\xi = \Delta\langle U \rangle / (d\langle U \rangle / d\xi)_{max}$. Figure 6(e) shows that the interface thickness becomes smaller as u_κ decreases. When u_κ decreases from $u_\kappa/U_{CL} = 0.9$ to 0.6, $\Delta\langle U \rangle$ increases gradually from 0.14 to 0.2, while $\Delta\xi$ decreases from 0.09 to 0.04, indicating that the velocity jump at the UMZ interface is larger over a smaller interface thickness. Figure 6(f) shows the profile of azimuthal vorticity $\Omega_\theta = \partial V_r / \partial x - \partial U / \partial r$ against ξ for cores defined at $u_\kappa/U_{CL} = 0.9$ and 0.95, similar to figure 6(a). The conditional averaged azimuthal vorticity $\langle \Omega_\theta \rangle$ peaks at the core interface and remains significantly low inside the core, consistent with the channel flow results (Kwon *et al.* (2014); Yang *et al.* (2016)).

Vortical structures

The peaked azimuthal vorticity at the interface leads to the observations in channel and TBL where strong shear are induced by concentrated vortices found on the interface (Yang *et al.* (2016); de Silva *et al.* (2017)). Figure 7 shows the azimuthal vorticity contours from the same snapshot, superpositioned with two core interfaces defined at $u_\kappa/U_{CL} = 0.8$ and 0.9. The colour axes of the vorticity contours are adjusted to visualise vortices with different strength more clearly. In the mid-planes, interfaces folds and contort for a persistent attachment to vortices with similar vorticity, indicating close correlation between the interface contortion and the azimuthal vortices. Cores closer to the wall have interfaces attached to stronger but smaller vortices, as shown in figure 7(b), consistent with figure 6(d) where $\Delta\xi$ is smaller for cores at lower u_κ values.

Figure 8 shows the average ratio between the population of prograde and retrograde vorticity at the vicinity of a three-dimensional (3D) interface defined at $u_\kappa/U_{CL} = 0.9$ against ξ. Slight away from the interface outside the core for $\xi < -0.1$, the ratio between the population of Ω_θ^+ and Ω_θ^- is fairly constant ($\approx 6:4$) with more prograde vortices over retrograde vortices. When approaching the interface at $\xi = 0$, there is an increase in prograde vortices accompanied with reduction on retrograde vortices to a maximum ratio approximately $9:1$. The ratio recovers back to a relatively constant and lower value after entered the core towards the pipe centre. The peaked population of prograde vortices and minimum retrograde vortices at the interface matches the channel flow results by Yang *et al.* (2016). These results indicate that the spatial contortion of the core interface strongly correlates to the azimuthal vortices with a dominant influence from the prograde vortices.

CONCLUSION

The quiescent core region is investigated in a turbulent pipe flow using DNS data at $Re_\tau = 500$. Multiple cores defined at varying threshold of streamwise velocity are studied for their characteristics and structural arrangement compared to TBL for the first time. The sharp change in streamwise velocity across the core interface accompanied by the peaked azimuthal vorticity is found in pipe similar to channel and TBL. The magnitude of the velocity jump at the interface is a function of wall-normal location, being larger nearer the wall similar to TBL by de Silva *et al.* (2017). Cores defined at lowered velocity thresholds expand towards the wall with reducing wall-normal distance between each other so that they are more closely distributed nearer the wall. This matched findings in turbulent boundary layer by de Silva *et al.* (2017) for a hierarchical distribution. The core interfaces themselves have thickness and is also thinner nearer the wall.

The pipe core exhibits thinning, thickening and meandering behaviour seen in turbulent boundary layer and channel flows, and can leave the pipe centreline outside the core. The intermittency in which the centreline is outside the core decrease for cores defined at lowered threshold velocity as they are thicker in average. The intermittency in pipe is slightly lower to channel for a core defined at the same velocity threshold. The core interface folds intensively. Visualisations show that the core interface contorts as a result from its persistent attachment to azimuthal vortices. The dominance of prograde vortices over retrograde vortices at the closer vicinity of the interface suggest that the spatial contortion of the interface is characterised by the prograde vortices.

REFERENCES

Adrian, R., Meinhart, C. & Tompkins, C. D. 2000 Vortex organisation in the outer region of the turbulent boundary layer. *Journal of Fluid Mechanics* **422**, 1–54.

Antonia, R. A., Teitel, M., Kim, J. & Browne, L. W. B. 1992 Low-Reynolds-number effects in a fully developed turbulent channel flow. *Journal of Fluid Mechanics* **236**, 579–605.

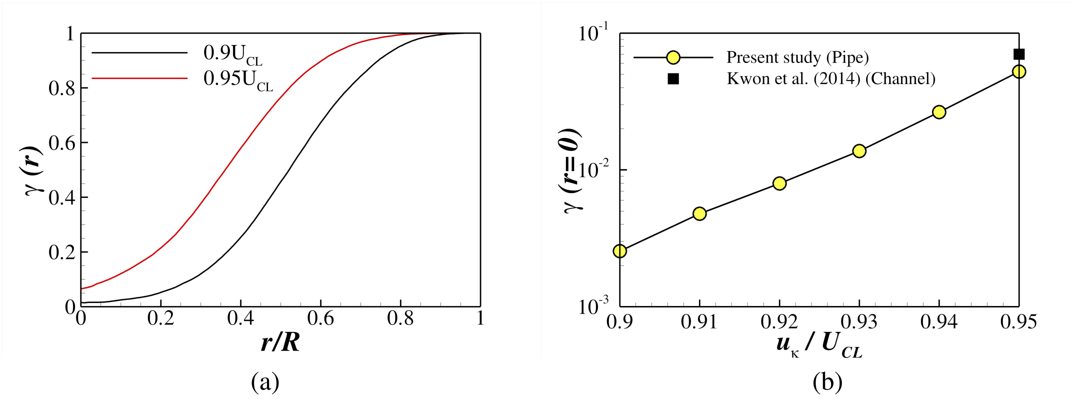

Figure 5. (a) Intermittency $\gamma(r)$ for cores defined at $u_\kappa/U_{CL} = 0.9$ (black) and 0.95 (red). γ represents the percentage of time that the flow spends outside of the core. (b) Centreline intermittency $\gamma(r=0)$ for a velocity threshold range of $0.9 \leq u_\kappa/U_{CL} \leq 0.95$.

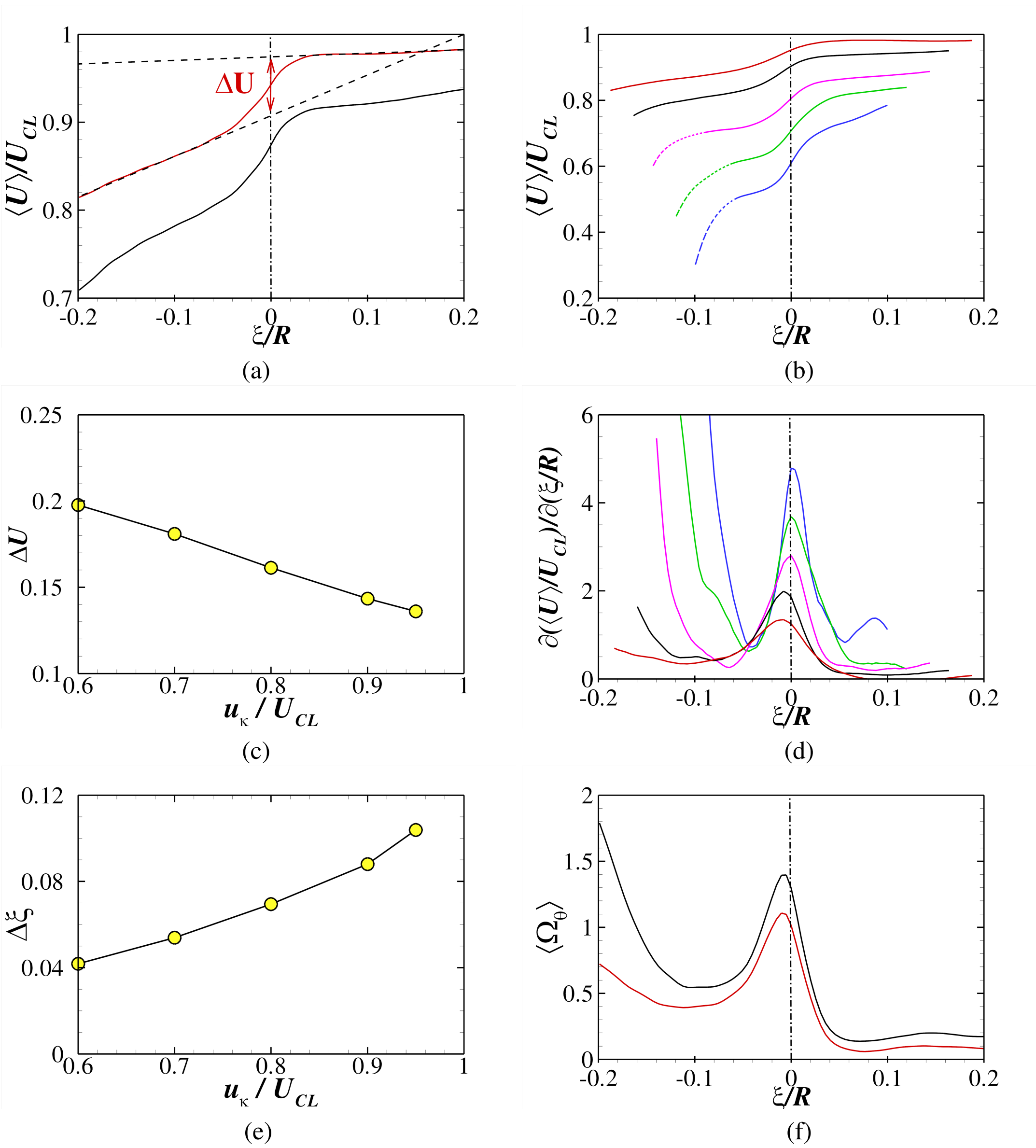

Figure 6. Conditional average of (a,b) streamwise velocity U as functions of distance from the interface ξ. $\xi > 0$ represents region inside the core. (c) Magnitude of the velocity jump across the interface ΔU (illustrated in (a)) for cores defined at five threshold velocities u_κ. (d) Velocity gradient $\partial\langle U\rangle/\partial\xi$ against ξ. (e) Core interface thickness ($\Delta\xi$) at five u_κ values. (f) Azimuthal vorticity Ω_θ against ξ. In (a,b,d,f), the profiles are for cores defined at $u_\kappa/U_{CL} = 0.95$ (red), 0.9 (black), 0.8 (magenta), 0.7 (green) and 0.6 (blue).

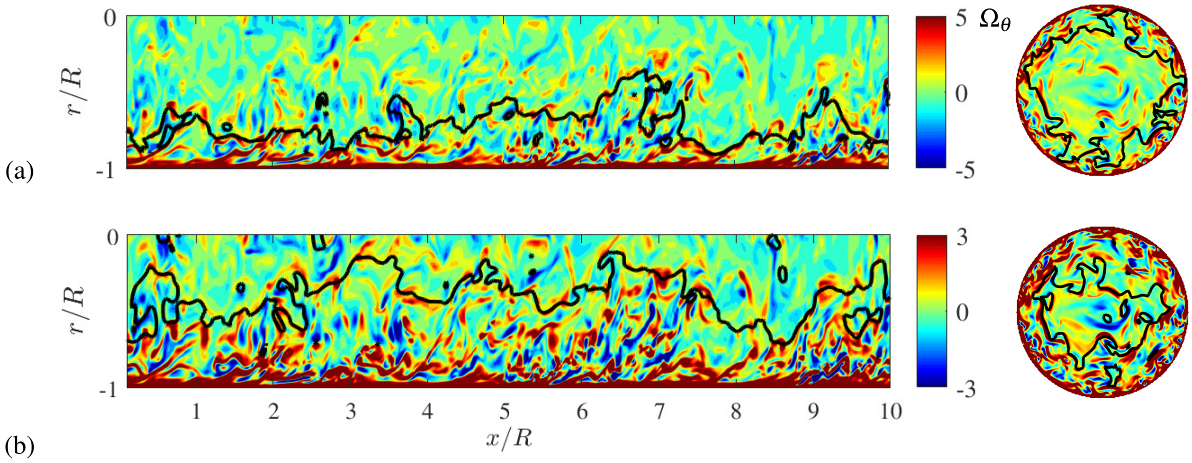

Figure 7. 2D Contours of azimuthal vorticity Ω_θ in the mid-plane and the cross-stream planes, super-positioned with the quiescent core interface defined at (a) $u_\kappa/U_{CL} = 0.8$ and (b) $u_\kappa/U_{CL} = 0.9$ for the same snapshot. The background contours of Ω_θ in (a) and (b) differ from the colour axis for clearer visualisation of vortices at difference strength.

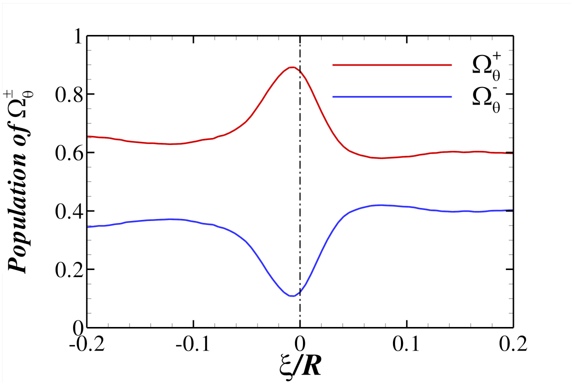

Figure 8. Ratio of the population (occurrence) between prograde and retrograde azimuthal vorticity, Ω_θ^+ and Ω_θ^- near a 3D core interface defined at velocity threshold $u_\kappa/U_{CL} = 0.9$ against distance from the interface ξ.

Eisma, J., Westerweel, J, Ooms, G. & Elsinga, G. E. 2015 Interfaces and internal layers in a turbulent boundary layer. *Physics of Fluids* **27**, 055103.

El Khoury, G. K., Schlatter, P., Noorani, A., Fischer, P. F., Brethouwer, G. & Johansson, A. V. 2013 Direct numerical simulation of turbulent pipe flow at moderately high Reynolds numbers. *Flow, Turbulence and Combustion* **91** (3), 475–495.

Fischer, P. F., Lottes, J. W. & Kerkemeier, S. G. 2008 nek5000 Web page. Http://nek5000.mcs.anl.gov.

Jung, S. Y. & Chung, Y. M. 2012 Large-eddy simulations of accelerated turbulent flow in a circular pipe. *International Journal of Heat and Fluid Flow* **33** (1), 1–8.

Kwon, Y. 2016 The quiescent core of turbulent channel and pipe flows. PhD thesis, University of Melbourne.

Kwon, Y. S., Philip, J., de Silva, C. M., Hutchins, N. & Monty, J. P. 2014 The quiescent core of turbulent channel flow. *Journal of Fluid Mechanics* **751**, 228–254.

Laskari, A., de Kat, R., Hearst, R. J. & Ganapathisubramani, B. 2018 Time evolution of uniform momentum zones in a turbulent boundary layer. *Journal of Fluid Mechanics* **842**, 554–590.

Meinhart, C. D. & Adrian, R. J. 1995 On the existence of uniform momentum zones in a turbulent boundary layer. *Physics of Fluids* **694** (7), 694–696.

Saxton-Fox, T. & McKeon, B. J. 2017 Coherent structures, uniform momentum zones and the streamwise energy spectrum in wall-bounded turbulent flows. *Journal of Fluid Mechanics* **826**, R6. doi:10.1017/jfm.2017.493.

de Silva, C. M., Hutchins, N. & Marusic, I. 2016 Uniform momentum zones in turbulent boundary layers. *Journal of Fluid Mechanics* **786**, 309–331.

de Silva, C. M., Philip, J., Hutchins, N. & Marusic, I. 2017 Interfaces of uniform momentum zones in turbulent boundary layers. *Journal of Fluid Mechanics* **820**, 451–478.

Wang, Z., Orlu, R., Schlatter, P. & Chung, Y. M. 2018 Direct numerical simulation of a turbulent 90 degrees bend pipe flow. *International Journal of Heat and Fluid Flow* **73**, 199–208.

Yang, J., Hwang, J. & Sung, H. J. 2016 Structural organization of the quiescent core region in a turbulent channel flow. *International Journal of Heat and Fluid Flow* **27**, 055103.

Yang, J., Hwang, J. & Sung, H. J. 2017 Influence of low- and high-speed structures on the quiescent core region in a turbulent pipe flow. Proceedings of the Tenth International Symposium on Turbulent and Shear Flow Phenomena.